JOURNAL OF MATERIALS SCIENCE 25 (1990) 3731–3738

Characterization of engineering ceramics by indentation methods

M. DIETZ, H.-D. TIETZ
Ingenieurh Hochschule Zwickau, Dr-Friedrichs-Ring 2a, 9540 Zwickau GDR

The induction of indentations in brittle materials and their evaluation result in information useful for the characterization of materials. In addition to the fracture-mechanical evaluation of the indentations, i.e. of the incipient cracks resulting from them, the cracks may be used for determining the fracture toughness,information regarding the hardness, critical size of surface defects, characteristic quantities of crack propagation, durability, as well as existing internal stresses.

1. Introduction

The expected use of ceramic materials in the field of mechanical engineering necessitates the development or modification of testing methods based on mechanical and non-destructive techniques for the comprehensive characterization of materials. In this context, it is important to use to its fullest extent the information obtained from each testing technique. A well-known technique used for evaluating the performance of brittle materials, including engineering ceramics, is connected with the induction of indentations (Vickers or Knoop indentor) and their evaluation, mainly for the determination of hardness and fracture-mechanical characterization. Partly, it also offers the possibility to draw conclusions concerning other material characteristics. The aim of this paper is to review the processes which take place during the penetration of an indentor and the information resulting from this for the characterization of materials, and to present the experimental results obtained for different Al_2O_3 materials.

2. Indentation techniques

2.1. The indentation process and crack formation

In contrast to metallic materials, such as steels, in the non-hardened state, where the indentation process of an indentor is mainly characterized through plastic deformation in connection with dislocation movements, the indentations in brittle materials are formed by deformation mechanisms in the microrange (plastic deformation, compaction of the structure) under the influence of multiaxial stress states leading to the formation of a so-called plastic zone below the indentor (see Fig. 1). The mechanisms responsible for the formation of the plastic zone below the indentor are principally not understood, although, from some investigations, for instance, an intensified dislocation movement (MgO, Al_2O_3, SiC), grain-boundary cracks due to slipping processes (ZnS) and localized shear bands (glass, KCl, LiF) are known [1]. Outside the plastic zone, strong elastic deformations occur in the vicinity of the indentation. The internal stresses, $\sigma_I^{E'}$ and σ_I^E, occurring in connection with this elastic–plastic deformation are responsible for the crack formation and crack growth at the indentors [1–7]. The analysis of the stress state due to the penetration of an indentor is of decisive importance in the discussion of the crack formation. This stress state can be described by two superimposed components. These components are a reversible and an irreversible (residual) component.

The reversible component, $\sigma_I^{E'}$, of the internal stress state is tied to the penetration process of the indentor (Fig. 1c); it acts outside the plastic zone ($r \geqslant b$) and can create compressive as well as tensile stresses [7]. However, the decisive contribution to the final crack configuration is made by the internal stresses, σ_I^E, in connection with the plastic zone below the indentor, and by the residual forces, F_I^E, present after relieving the stress (Fig. 1d).

Crack formation due to the penetration of a Vickers diamond into the surface of a brittle material, despite slightly different interpretations and terminology in the literature, is shown schematically in Fig. 1 which illustrates the existing crack types. After relieving the stress, the following crack types (Fig. 1a) can be detected.

2.1.1. Diagonal cracks

Starting from the corner points of the Vickers indentation, when the diagonal is extended, cracks are observed, which are orientated perpendicular to the surface and which are termed diagonal cracks. In principle, two kinds must be distinguished, diagonal cracks which start from the corners and propagate to a relatively low depth (approximately in the depth of the indentation), the so-called Palmquist cracks (Fig. 1b), and diagonal cracks which propagate below the plastic zone and which are designated radial cracks.

Palmquist cracks are characteristic of some groups of materials having a high toughness such as WC, WC/Co alloys, and they preferably occur at low

0022–2461/90 $03.00 + .12

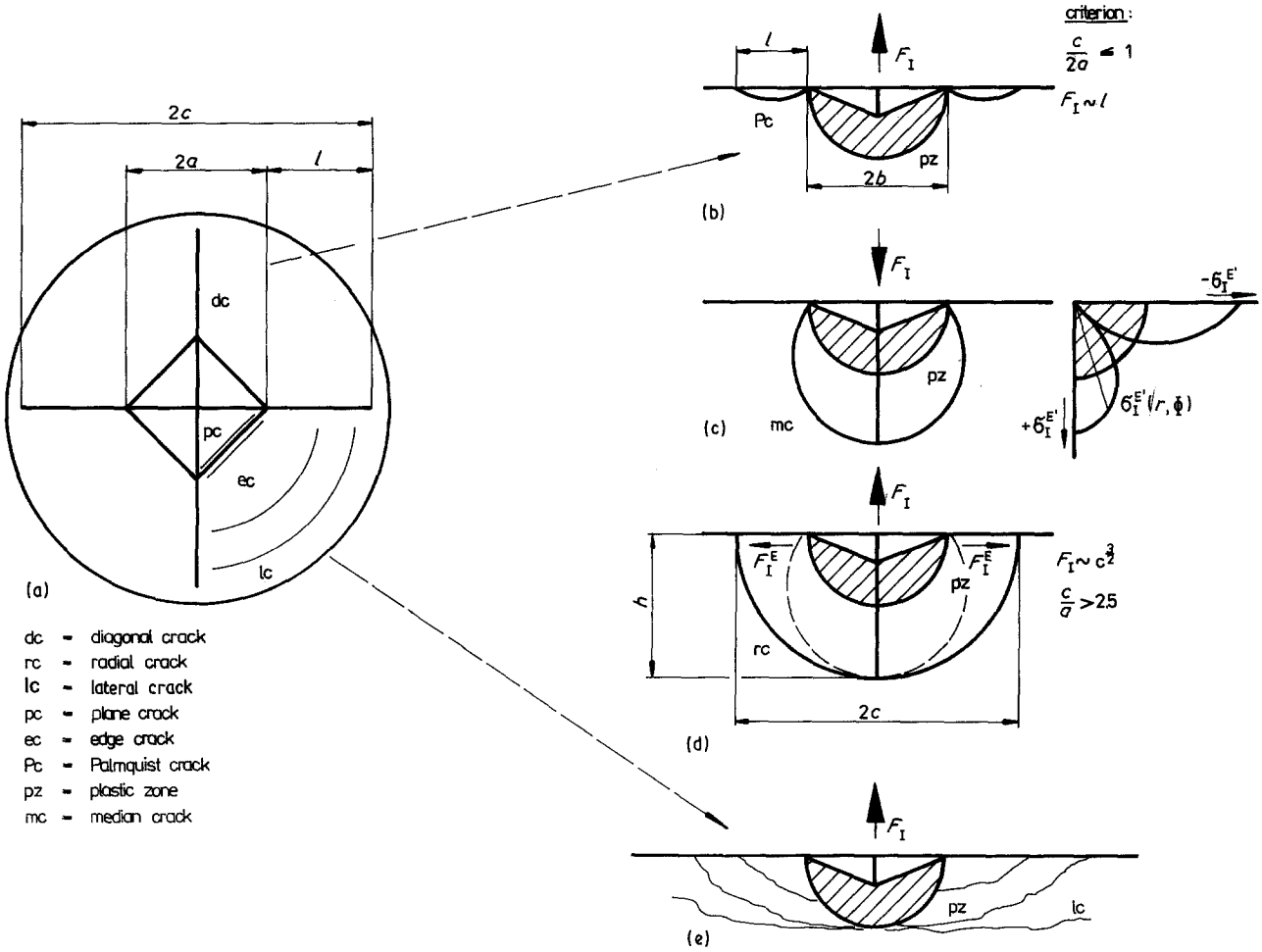

Figure 1 Schematic view of the crack formation at a Vickers indentation [3, 4, 7, 8, 12, 15, 28].

indentation forces with the surface state (roughness) and "indentor radius" also being important.

The following criteria are given for characterizing Palmquist cracks:

$$0.25 \leqslant l/a \leqslant 2.5 \quad (1)$$

$$c/a \leqslant 1 \quad (2)$$

$$F_I \sim l \quad (3)$$

where F_I is the indentor force, c and l are the crack lengths. Depending on the material, radial cracks are formed during the penetration of the indentor on the basis of an irreversible deformation (plastic zone) which is the cause of crack formation (median crack, Fig. 1c) in the region having the highest stress concentration directly below the indentor, under the influence of a critical indentor force, F_{Ic}, or/and during the relief through the action of the field of residual stresses (Fig. 1d). Radial cracks, which exclusively result from the action of the internal stresses due to the plastic zone σ_I^E, can have different shapes, which represent, depending on the indentor force F_I, transitional shapes between a Palmquist crack and a semicircular crack ("half-penny shaped crack").

The following relationships are used for the determination of the existence of radial cracks

$$F_I \sim c^{3/2} \quad (4)$$

$$c/a \geqslant (2) \ldots (2.5) \ldots (3) \quad (5)$$

[2, 5, 8, 9]. Investigations made by Jones *et al.* [10] indicate that there is a dependency of the magnitude of the ratio c/a on the material (Al_2O_3: $c/a = 2$, $F_{IHV} = 49\,N$, $ZrO_2 + Y_2O_3$ $c/a = 3$, $F_{IHV} = 530\,N$).

2.1.2. Lateral cracks

2.1.2.1. Side edge and side face cracks. Experimental studies of Marshall [1] on the mechanism of crack formation in soda-lime glass (*in situ* observations) yielded the following essential findings ($F_{IHV} = 90\,N$).

(i) The final crack configuration is formed during the removal of the indentor from the surface (continuous growth of the radial cracks until complete relief is reached, formation of the lateral cracks after complete relief has been reached).

(ii) After the relief, a high amount of internal stress still remains. An indication of this is the existence of stress-induced birefringence.

The above considerations essentially refer to crack formation using a Vickers indentor. The mechanism of crack initiation through a Knoop indentor, having the advantage that only one crack is formed, has the same importance. With Knoop indentors, in principle, the same mechanisms of crack formation can be assumed to exist. A schematic representation of the crack structure to be expected is shown later in Fig. 4.

2.2. Characterization of materials

2.2.1. Fracture toughness

Although Palmquist [11], using Vickers indentors, proved in 1962, through investigations on tungsten

carbides, that there is a relationship between the crack length and toughness, this fact received relatively little attention in investigations of ceramic materials. Not until the mid seventies, did this observation receive more attention, and a number of fundamental studies were then performed on the indentation fracture mechanics in ceramic materials and glasses using "sharp" indentors, and on the fracture-mechanical evaluation of the crack formation and crack growth on the basis of the linear-elastic fracture mechanics [1–3, 6, 8, 12–14].

With the help of different models of crack formation at indentations, and also of empirical relationships, various formulations for the determination of the fracture toughness are given. In connection with the mechanism of crack formation described above, assuming that the stress intensity factor $K_I > K_{Ic}$, we obtain as fracture criterion the critical stress intensity factor, K_{Ic}, from the crack length (indentation/crack length or ICL) method [1, 5, 7, 12, 13]

$$K_{Ic} = 0.016(E/HV)^{1/2} F_{IHV} c^{-3/2} \quad (6)$$

and

$$K_{Ic} = 0.022\,(E/HK)^{1/2} F_{IHK} c^{-3/2} \quad (7)$$

where E is Young's modulus, HV Vicker's hardness, HK Knoop hardness, $F_{IHV,HK}$ the indentor force, and c the crack length.

For existing radial cracks, the following relationships are also known

$$K_{Ic} = 0.067 \left(\frac{c}{a}\right)^{-3/2} HV a^{1/2} \left(\frac{E}{HV}\right)^{2/5} \text{[15]} \quad (8)$$

$$K_{Ic} = 0.16\, HV a^{1/2} (c/a)^{-3/2} \text{[16]} \quad (9)$$

$$K_{Ic} = 10^{Y} (E/HV)^{2/5} HV a^{1/2} \text{[17]} \quad (10)$$

$$[Y = -1.59 - 0.34 \lg x - 2.02 (\lg x)^2 + 11.23 (\lg x^3) - 24.97 (\lg x)^4 + 16.32 (\lg x)^5]$$

$$x = c/a$$

$$K_{Ic} = \frac{F_{IHV}}{(\pi c)^{3/2} \tan \beta} \text{[9]} \quad (11)$$

$$K_{Ic} = 0.028\,(E/HV)^{1/2}\, HV a^{1/2} (c/a)^{-3/2} \text{[7]} \quad (12)$$

$$K_{Ic} = 0.028\,(E/HV)^{2/5}\, HV a^{1/2} \lg (8.4a/c) \text{[18]} \quad (13)$$

In the literature, the following formulations are used for Palmquist cracks

$$K_{Ic} = 0.018 \left(\frac{l}{a}\right)^{-1/2} HV a^{1/2} \left(\frac{E}{HV}\right)^{2/5} \quad (14)$$

$$K_{Ic} = 0.0788 \left(\frac{HV\, F_{IHV}}{l}\right)^{1/2} \quad (15)$$

On the basis of these formulations, Moussa *et al.* [19] investigated the comparability of the individual relationships with each other and with the results of other testing techniques (Fig. 2) for HPSiC (aluminium content 1.5%). For the range of testing forces investigated, qualitatively the same dependencies were found, with deviations between the different relationships of up to 100% being possible, however. Up to an indentor force of $F_I = 50$ N, an increase in K_{Ic} is found, and above this force, there is only a small decrease or an almost constant behaviour. The cause of this behaviour in the case of higher indentor forces is the inclusion of a relatively high number of crystals connected with the fracture region, so that the influence of local events (microstructure–crack size ratio) decreases. Existing comparative values for the K_{Ic} values, obtained by means of the notched beam (NB) method and indentation/strength in bending (ISB) method are within the scattering range of the relationships of the ICL method.

When the stress σ_I^E is superposed by an additional stress, σ_i (external stress σ_a, internal stress σ^E), the following equation applies

$$K_I = \sum_i \sigma_i (\pi c)^{1/2} Y + \kappa_I F_I c^{-3/2} \quad (16)$$

where $\kappa_I = 0.016\,(E/HV)^{1/2}$ for Vickers indentors, and Y is the crack geometry factor ($Y = 2/\pi$).

From Equation 16, a relationship can be derived which allows the determination of the fracture toughness by means of a bending load after indentations have been induced (ISB method)

$$K_{Ic} = v\, 0.683\, (E/H)^{1/8} (\sigma_{bBD} F_I^{1/3})^{3/4} \quad (17)$$

where $v = 0.86$ [20].

2.2.2. Internal stresses

Under the action of internal stresses, using Equation 16 we get

$$K_{Ic} = \sigma^E (\pi c)^{1/2} Y + \kappa_I F_I c^{-3/2} \quad (18)$$

On the one hand, Equation 18 describes the influence of internal stresses on K_{Ic}, but it also allows the determination of existing internal stresses, provided "internal-stress-free" K_{Ic} values are known.

Marshall and Lawn [21] utilize this fact for the determination of residual surface stresses by analysing the crack geometry in connection with Vickers indentations, with stressed and stress-free soda-lime glass being used in the investigation.

Assuming a biaxial compressive stress state, the following equation applies

$$(F_I c^{-3/2})_{\sigma^E} = (F_I c^{-3/2})_0 \left(1 - \frac{2Z\sigma^E c^{1/2}}{\pi^{1/2} K_{Ic}}\right) \quad (19)$$

where $(F_I c^{-3/2})_0 = K_{Ic}/\kappa_I$ = constant. The indices σ^E

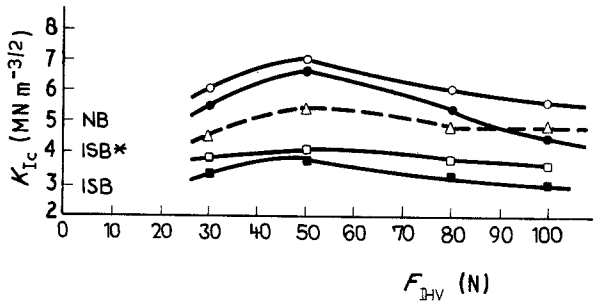

Figure 2 Fracture toughness K_{Ic} (ICL) plotted against indentor force F_I for HPSiC (comparison of K_{Ic} (NB), K_{Ic} (ISB) – ISB*: annealed specimen, $F_{IHK} = 30$ N) [19]. (●) [16], (○) [17], (□) [6], (△) [18], (■) [7].

and 0 characterize the stressed and unstressed state, respectively, Z is a constant having unit value in the range of the crack depth, provided surface defects and stress gradients are neglected. If $(F_I c^{-3/2})$ is plotted against $c^{1/2}$ and $(F_I c^{-3/2}) \neq f(c^{1/2})$, then the unstressed state $(F_I c^{-3/2})_0$ exists, and when $(F_I c^{-3/2}) = f(c^{1/2})$, then the specimen is stressed $[(F_I c^{-3/2})_{\sigma E}]$.

2.2.3. Critical defect size

On the basis of the relationship $F_I \sim c^{3/2}$, the defect size can be purposely modified by varying the indentor force, which results in a defect size that, in case of a bending load on the tensile side, no longer initiates fracture at the indentation, i.e. material-inherent defects predominate. According to Ikeda and Igaki [22], the critical defect size can also be obtained by comparing the fracture stresses of damaged and undamaged specimens.

2.2.4. Crack propagation characteristics, durability

A number of works [14, 23, 24] give theoretical and experimental possibilities for the detection of the dynamic and static failure on specimens damaged by indentations. Cook and Lawn [24] show that, provided $K_I < K_{Ic}$, the crack kinetics can be described as

$$v = v_0 (K_I / K_{Ic})^n \quad (20)$$

where v_0 and n are material constants.

The problem of the dynamic failure ($\dot{\sigma}_a = \sigma_a / t =$ constant) is described by the combination of Equations 6 and 20

$$\frac{dc}{dt} = v_0 [\kappa_I F_I / K_{Ic} c^{3/2} + \pi^{1/2} Y \dot{\sigma}_a c^{1/2} t / K_{Ic}]^n \quad (21)$$

The dynamic failure strength, σ_{bBD}, is obtained by means of the following relationships

$$\sigma_{bBD} = (\varepsilon' \dot{\sigma}_a)^{1/(n'+1)} \quad (22)$$

with

$$n' = 3n/4 + \tfrac{1}{2} \quad (23)$$

and

$$\varepsilon' = (2\pi n')^{1/2} \sigma_{BD}^{n'} c / v_0 \quad (24)$$

Investigations under inert conditions show, for example, for various glasses, Al_2O_3, SiC, piezo and glass ceramics, that the characteristics of crack propagation, n and v_0, can be obtained by means of the above relationships in combination with the graphical determination of n' and by plotting σ_{bBD} against $\dot{\sigma}_a$. The results obtained in this way are shown for soda-lime glass in Fig. 3. Furthermore, it becomes possible to determine the expected service life in the case of static loads.

2.2.5. Hardness

In addition to the fracture-mechanical evaluation of the cracks formed at the indentations, the size of the indentation itself is an important quantity for the determination of the hardness, with the resulting cracks being a disadvantage, however, because they affect the test result. In order to achieve crack-free indentations, i.e. true results, only small testing forces may be used for the measurement, at which forces the hardness depends on the testing force, as shown by the investigations in item 3 (Fig. 4). Because of this and due to further disadvantages of the conventional hardness measurement methods using Vickers or Knoop indentors, engineering ceramics require test methods which allow a measurement under load and which are free from subjective influencing factors. Here, the recording hardness measurement, which allows the determination of a hardness index, L_2VH (irrespective of the indentor force and crack formation), and the hardness measurement by means of the ultrasonic contact impedance (UCI) method [25, 26] are important.

The UCI method also uses a Vickers pyramid as indentor and measures the hardness under the effect of the testing force. The increase in the resonance frequency of a probe whose tip holds the Vickers indentor forms the basis of this method, and the change in

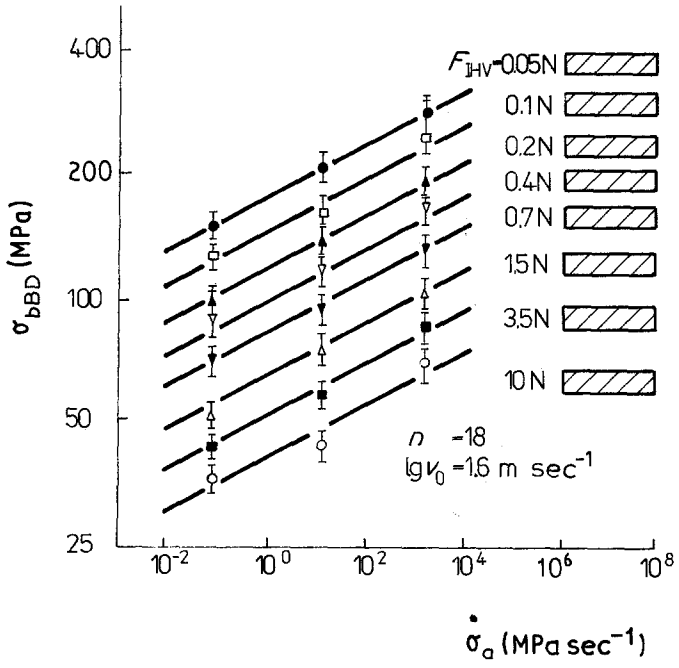

Figure 3 Relationship between bending fracture strength (indentation) σ_{bBD} and speed of stress increase, $\dot{\sigma}_a$ [24], for soda-lime glass.

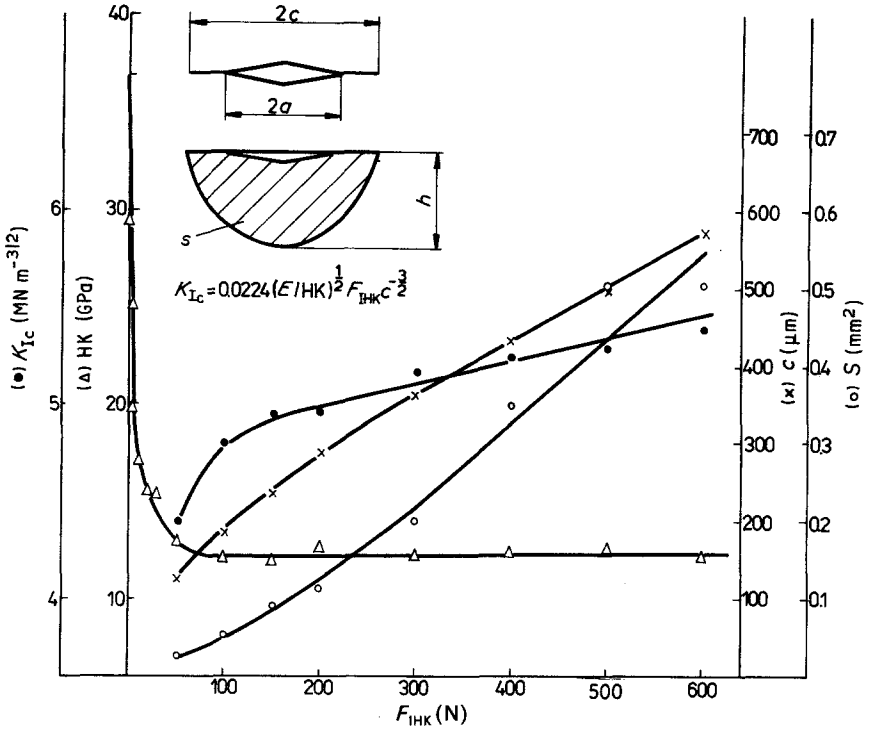

Figure 4 Influence of the indentor force, F_I, on hardness, fracture toughness, crack length and crack area: material A1 (Al_2O_3).

the frequency is a measure of the surface of the indentation and, therefore, of the hardness of the material. In this method, a testing force $F_I \approx 10\,N$ and an impact velocity $v_I \approx 0.3\,mm\,sec^{-1}$ are used [26]. The change in the resonance frequency of the oscillating bar, Δf, also depends on the Young's moduli of the indentor, E_I, and specimen, E_p, resulting in material-specific calibration functions. The Vickers hardness is calculated according to the following equation

$$HV_{UCI} = HV'_{UCI}\left(\frac{1/E_N + 1/E_I}{1/E_P + 1/E_I}\right) \quad (25)$$

From this equation, it becomes obvious that the Young's modulus of the indentor, E_I, specimen, E_P (to be obtained by means of other methods such as ultrasonic velocity measurement, resonance frequency method), or of a comparison standard, E_N (e.g. hardness reference plate) is required for the determination of HV_{UCI} in order to correct the indicated value for HV_{UCI} accordingly. On the other hand, it should also be possible to determine the Young's modulus of the specimen when the hardness is known. This procedure could be used as a supplementary method in the testing of engineering ceramics.

3. Experimental investigations

3.1. Materials

The experimental results described below refer exclusively to various Al_2O_3 materials which can be characterized by the values listed in Table I. The aluminium content is $\geqslant 99\%$ for materials A1, A2 and A6, $\approx 97.5\%$ for A4 and $\approx 94.8\%$ for A5. The specimens were 10 mm × 20 mm × 100 mm in size for material A1 and 4 mm × 5 mm × 45 mm for all other materials.

3.2. Test procedures

The indentations (Vickers or Knoop indentor) used for evaluating the crack length are made in polished surfaces (transverse polish of bend specimens) using a small-load hardness tester 3202 (Zwick). The indentations were induced into bend specimens which were in an unmachined state. Hardness was measured using a Microdure instrument (Krautkrämer) according to the UCI method. The flexural load was applied in a four-point bending test with the spacing of the supports $s_1 = 20\,mm$ and $s_2 = 40\,mm$ and a cross-head speed of $v_F = 0.5\,mm\,min^{-1}$, unless a purposeful variation of $\dot{\sigma}_a$ was required. In case of three-point bending, the support spacing was $s = 25\,mm$. A general purpose strength testing machine of the Fu 10 000 eZ type was used as testing machine.

TABLE I Characteristic values of the material (Al_2O_3)

Material	Density ($g\,cm^{-3}$)	E (GPa)	σ_{4bB} (MPa)	m	HV 5 (GPa)	K_{Ic} ($MN\,m^{-3/2}$)			HV_{UCI} (GPa)
						NB	ISB	ICL	
A1	3.89	380	–	–	14.67	–	–	3.49	–
A2	3.56	264	135	7.8	10.65	2.87	2.72	3.04	5.64
A5	3.88	353	248	6.5	15.8	4.02	3.82	3.95	15.7
A6	3.96	396	205	3.6	18.21	3.95	3.94	3.26	16.46
A4	3.79	345	215	10.4	13.33	4.05	3.43	3.55	13.64

3.3. Results and discussion

Fig. 4 shows the experimental results of the relationship between fracture toughness, K_{Ic} (ICL), Knoop hardness, HK, crack length, c, or crack area, S, and indentor force, F_I (Knoop indentor). It can be seen that the Knoop hardness very much depends on the force in the range of small indentor forces and shows an almost constant behaviour at forces $F_I \geqslant 49$ N for the material used. The same results are found for Vickers indentors and in hardness measurements. The resulting crack length, c, corresponds to the relationship

$$F_I = 0.0228\ c^{1.6} \qquad (26)$$

and therefore, it agrees with the behaviour of $F_I \sim c^{3/2}$ which is expected according to theory. On the basis of Equation 7, the behaviour of K_{Ic} (ICL), which can be seen in Fig. 4, was calculated, and in the range of small forces, a clear dependency of the indentor force was also found, which may be caused, on the one hand, by the testing-force dependency of the hardness and, on the other hand, by an incompletely developed radial crack. Furthermore, the existing radial cracks serve as model flaws for the non-destructive material testing (e.g. ultrasonic flaw detection, penetration method). Therefore, the calibration curves based on Equation 26 or on the relationship $F_I \sim S$, which can be derived from it, are important. However, semicircular cracks, i.e. $c = h$ ("half-penny"-shaped cracks) were assumed for the calculation of S.

Fig. 5 illustrates the dependency of K_{Ic} (ISB) and of the related bending fracture strength, σ_{bBD} (unpolished specimens) on the indentor force, F_I (Vickers indentor). K_{Ic} (ISB) was calculated according to Equation 17. Here, in the range of small indentor forces ($F_I < 49$ N), a clear dependency of the fracture toughness on the indentor force also became evident. For indentor forces $F_I \geqslant 49$ N, an almost constant behaviour is found, which was also observed for the investigated range up to $F_I = 980$ N. However, especially in the case of a four-point bending load, it was observed that a certain material-dependent crack length, c, is required to initiate the fracture at the indentation. Thus, a certain defect size (crack length) must be exceeded to suppress the influence of natural material-inherent defects. Material A5 investigated in this paper requires an indentor force of $F_I = 20$ to 50 N, i.e. $2c \approx 162\,\mu$m, to ensure that the fracture occurs at the indentation. In this manner, by bending, a critical size of surface defects must be determined for each material on the tensioned width. To enable comparison, Fig. 5 shows the K_{Ic} values (ICL) calculated according to Equations 6 and 8 to 13 for an indentor force of $F_I = 49$ N. A good agreement between the values calculated from Equation 6 and the K_{Ic} (ISB) values was observed. Furthermore, comparison with results obtained on notched specimens (notched beam) is possible. The specimens notched by a saw (diamond wheel $N \approx 170\,\mu$m) possess K_{Ic} (NB) values which are somewhat higher than those obtained for specimens machined by a laser ($N \approx 20$ to $30\,\mu$m), which is caused by the notch width. The specimens notched by a saw also show a very good agreement with the K_{Ic} (ICL) and K_{Ic} (ISB) values if $F_I \geqslant 49$ N. It becomes evident that indentor techniques are suited for the determination of the fracture toughness of ceramics, and that they provide results comparable to those for notched specimens. This can be seen in Table I for the other materials examined.

Furthermore, with the ISB technique, the effect of the trasverse speed, v_F, or of the speed of stress increase, $\dot{\sigma}_a$, obtained from it on the bending fracture strength, σ_{bBD}, and fracture toughness, K_{Ic} (ISB), was investigated.

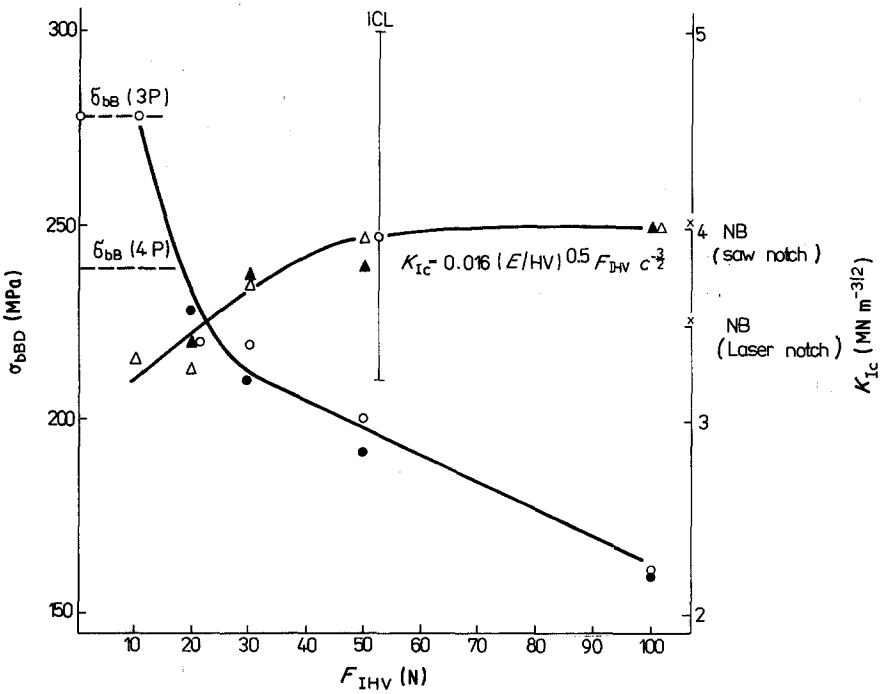

Figure 5 Dependence of bending fracture strength, σ_{bBD}, and fracture toughness, K_{Ic} (ISB), on the indentor force, F_I (Vickers indentor), and comparison of K_{Ic} values obtained by different methods: material A5 (Al_2O_3). (△) K_{Ic} (ISB–3P), (▲) K_{Ic} (ISB–4P), (○) σ_{bBD} (ISB–3P), (●) σ_{bBD} (ISB–4P).

TABLE II Influence of loading speed on σ_{3bBD} and K_{Ic} (ISB) material A5 (F_{HV} = 98 N)

v_F (mm min^{-1})	$\dot{\sigma}_a$ (MPa sec^{-1})	σ_{3bBD} (MPa)	K_{Ic} (ISB) (MN m$^{-3/2}$)
0.05	2.5	204	4.678
0.5	5.9	228	5.08
1.5	23.1	227	5.07
2.4	34.5	245	5.36

Table II reveals that the expected increase in σ_{3bBD} and K_{Ic} (ISB) occurs with increasing speed (see Fig. 3). This fact was used in calculating the crack propagation characteristics, v_0 and n, according to Equation 20 on the basis of Equation 21 to 23. For material A5, n = 22.8 and lg v_0 = 2.58 m sec^{-1} were calculated, which approximately correspond to the values known from the literature.

In addition to the investigations of the conventional hardness as a function of indentor force (see Fig. 4), the hardness of materials A2, A4, A5 and A6 are determined according to the UCI method (HV_{UCI}), with the calculation being based on Equation 25. These results are also included in Table I. In element testing, it is also important to find out to what extent there is a correlation between hardness measurement as a method which causes only little damage, and the other characteristics used for describing the mechanical behaviour of engineering ceramics. Fig. 6 shows that, on the basis of the mean values of the batches (see Table I), consideration of individual values results in excessive deviations, an almost linear relationship between the Young's modulus (determined from measurements of the ultrasonic speed [27]) and the density, ρ, and the bending fracture strength in the case of four-point loading, σ_{4bB}, can be obtained. This makes it possible to estimate the other material characteristics from measured hardness values, even if the individual characteristics result from procedures covering different cross-sectional parts of the specimens.

4. Conclusion

The induction of indentations in brittle materials, especially engineering ceramics, provides information useful for characterizing materials. In addition to the fracture-mechanical evaluation of the indentations, i.e. of the incipient cracks resulting from them, for a determination of the fracture toughness from the crack length (ICL technique) and in addition to their use as natural defects in subsequent bend loading (ISB technique), further conclusions regarding the identification of the materials can be drawn. The critical size of surface defects, as well as characteristic values required for the description of the crack propagation behaviour, and the durability can be determined from the crack length in connection with a bend loading. Furthermore, the hardness value can be calculated from the indentations (Vickers and Knoop indentors), with the conventional hardness being dependent on the testing force and falsified by existing cracks. The hardness measurement according to the UCI method allows the execution of measurements under load and is independent of subjective influences. The experimental results obtained for different Al_2O_3 materials indicate a relationship between the impedance hardness and Young's modulus, density, bending fracture strength and fracture toughness. Moreover, for these materials, the determination of these characteristic values on the basis of cracks existing at the indentations and information that can be derived from this, is shown.

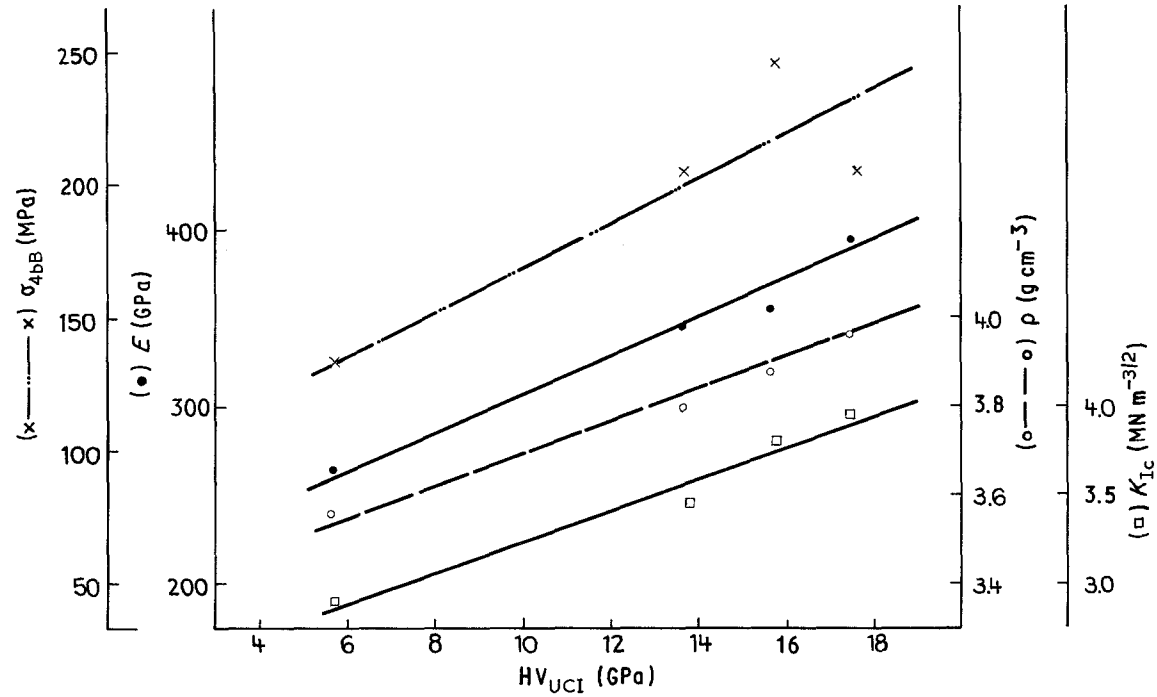

Figure 6 Relationship between bending fracture strength σ_{4bB}, Young's modulus, E, density, ρ, fracture toughness, K_{Ic} (ISB), and hardness, HV_{UCI}, using the UCI method.

References

1. D. B. MARSHALL, "Surface damage in ceramics: Implications for strength degradation, erosion and wear", in Progress in Nitrogen Ceramics, edited by F. L. Riley (Martinus Nijhoff, Boston, The Hague, Dordrecht, Lancaster, 1983) pp. 635–656.
2. B. R. LAWN and E. R. FULLER, *J. Mater. Sci.* **10** (1975) 2016.
3. D. B. MARSHALL *et al.*, *Proc. R. Soc. Lond. A* **385** (1983) 461.
4. J. G. P. BINNER and R. STEVENS, *J. Brit. Ceram. Soc.* **83** (1984) 168.
5. Y. MATSUO and A. NOZUE, *Bull. JSME* **27** (1984) 2360.
6. G. R. ANSTIS *et al.*, *J. Amer. Ceram. Soc.* **64** (1981) 533.
7. B. R. LAWN, A. G. EVANS and D. B. MARSHALL, *ibid.* **63** (1980) 574.
8. M. PETZOLD, "Modellierung der Radialrißentstehung in Umgebung von Mikrohärteeindrücken und deren Anwendung für Eigenspannungs- und Festigkeitsuntersuchungen von Glas Diss", (A) (MLU, Halle, Wittenberg, 1987).
9. K. H. ZUM GAHR, *Z. Metallkde* **69** (1978) 534.
10. S. L. JONES, J. NORMAN and R. SHAHANI, *J. Mater. Sci. Lett.* **6** (1987) 721.
11. S. PALMQUIST, *Arch. Eisenhüttenw.* **33** (1962) 629.
12. D. B. MARSHALL, *J. Amer. Ceram. Soc.* **67** (1984) 57.
13. J. J. PETROVICH, *J. Amer. Ceram. Soc.* **66** (1983) 277.
14. D. K. SHETTY, A. R. ROSENFIELD and W. DUCKWORTH, *Commun. Amer. Ceram. Soc.* **68** (1985) C-65.
15. K. NIIHARA, *J. Mater. Sci. Lett.* **2** (1983) 221.
16. A. G. EVANS and E. A. CHARLES, *J. Amer. Ceram. Soc.* **59** (1975) 371.
17. A. G. EVANS, ASTM–STP 678 (American Society for Testing and Materials, Philadelphia, Pennsylvania, 1979) p. 112.
18. K. NIIHARA, R. MORENA and D. P. H. HASSELMANN, *J. Mater. Sci. Lett.* **1** (1982) 13.
19. R. MOUSSA, J. COPPOLANI and F. OSTERSTOCK, *Proc. Brit. Ceram. Soc.* **32** (1982) 237.
20. P. CHANTIKUL *et al.*, *J. Amer. Ceram. Soc.* **64** (1981) 539.
21. D. B. MARSHALL and B. R. LAWN, *J. Amer. Ceram. Soc.* **60** (1977) 86.
22. K. IKEDA and H. IGAKI, *Commun. Amer. Ceram. Soc.* **70** (1987) C-29.
23. D. B. MARSHALL and B. R. LAWN, *J. Amer. Ceram. Soc.* **63** (1980) 532.
24. R. F. COOK and B. R. LAWN, *J. Res.* **89** (1984) 453.
25. F. FRÖHLICH and P. GRAU, Pat. WPGOI N/188 542 (1975).
26. C. KLEESATTEL, "Das UCI-Härteprüfverfahren", Sonderdruck 239, Krautkrämer GmbH.
27. H.-D. TIETZ and M. DIETZ, *AdW-DDR, Berlin, APK* **11** (1986) 56.
28. F. KROUPA and F. HNILICA, *Silikaty, Praha* **29** (1985) 157.

Received 9 December 1988
and accepted 23 August 1989